Original Research



Ex vivo modulation of tau phosphorylation by hyperpolarized light: implications for Alzheimer's disease therapy

Emiliana Piscitiello¹, Barbara Truglia^{2,3}, Sara Castria⁴, Alessandra Occhinegro¹, Elisa De Angelis¹, Luca Alberti¹, Ludovico Taddei¹, Timna Hitrec¹, Roberto Amici¹, Jack A. Tuszynski^{3,4}, Marco Luppi^{1*}

¹University of Bologna, Department of Biomedical and Neuromotor Sciences, Bologna, Italy, 40127.

- ² University of Alberta, Faculty of Engineering, Department of Biomedical Engineering, Edmonton, Canada, T6G 1H9.
- ³ University of Alberta, Faculty of Science, Department of Physics, Edmonton, Canada, T6G 2E1.
- ⁴ Politecnico di Torino, Department of Mechanical and Aerospace Engineering (DIMEAS), Turin, Italy, 10129.

*Correspondence: marco.luppi@unibo.it DOI: https://doi.org/10.56280/1714956796

This article is an open access article distributed under the terms and conditions of the Creative Commons Attributions (CC BY) license (https://creativecommons.org/licenses/by/4.0/)

Received: 31 August 2025 Accepted: 29 September 2025 Online Published: 30 September 2025

Abstract

Alzheimer's disease (AD) is characterized by amyloid-β accumulation and tau hyperphosphorylation, leading to neurodegeneration and cognitive decline. Photobiomodulation (PBM) has shown promise in mitigating AD pathology, yet its effects on tau remain poorly understood. We investigated the impact of high-polarized light (HPL; Bioptron Quantum Hyperlight, 350–3400 nm) on tau phosphorylation using an ex vivo rat brain slice model of synthetic torpor (ST), a reversible hypometabolic state inducing controlled tau hyperphosphorylation. Slices were incubated at physiological (37 °C) or hypometabolic (25 °C) temperatures and exposed to HPL for 10 or 20 minutes. Western blot analyses of Tau-1 (non-phosphorylated tau), p-GSK3\beta (Ser9), and p-T205 revealed that HPL increased Tau-1 levels in warm slices, indicating a shift toward reduced tau hyperphosphorylation. p-GSK3β modulation was variable, reflecting inter-animal differences and temperature-dependent kinase/phosphatase dynamics. Cold slices exhibited smaller, more heterogeneous responses, consistent with suppressed metabolic activity and attenuated PBM signaling. Site-specific p-T205 changes suggest transient kinase activation and redox signaling, compatible with an overall trend toward normalized tau phosphorylation. These results highlight how HPL can modulate tau phosphorylation ex vivo, with the most consistent effects under normothermic conditions. Despite limitations, our findings provide preliminary evidence supporting HPL/PBM as a potential therapeutic strategy for tauopathies. Future in vivo studies are warranted to elucidate mechanisms, optimize dosing, and explore glymphatic-mediated clearance in PBM-treated brains.

Keywords: photobiomodulation, hyperpolarized light, Alzheimer, hypothermia, synthetic torpor, tau hyperphosphorylation

1. Introduction

Alzheimer's disease (AD) is among the fastest-growing causes of death worldwide and, to date, remains without a cure. AD is a progressive neurodegenerative disorder that leads to severe cognitive decline through neuronal loss and synaptic dysfunction (Calabrò *et al.*, 2021). Its two major hallmarks are the extracellular deposition of amyloid- β (A β) plaques and the intracellular accumulation of hyperphosphorylated tau (PP-Tau) in the form of neurofibrillary tangles (NFTs) (Delacourte & Defossez, 1986; Karran et al., 2011; Goedert *et al.*, 2017).

Tau, a microtubule-associated protein, plays a central role in stabilizing microtubules and maintaining efficient axonal transport (Wang & Mandelkow, 2016; Lantero-Rodriguez et al., 2024). When excessively phosphorylated, Tau detaches from microtubules, loses its stabilizing function, and shows a strong tendency to aggregate first into oligomers and subsequently into NFTs—a pathological process shared by a group of neurodegenerative disorders collectively termed tauopathies (Gerson et al., 2016; Goedertv et al., 2017; Luppi et al., 2019). Several post-translational modifications are implicated in tau aggregation, but

implicated in tau aggregation, but phosphorylation is the predominant one: Tau contains 85 putative phosphorylation sites, 71 of which can be modified under either physiological or pathological conditions (Avila, 2006; Sergeant *et al.*, 2008).

Tau phosphorylation is tightly controlled by the phosphatases. between kinases and interplay Disruption of this equilibrium, either through increased kinase activity or reduced phosphatase function, results in abnormal hyperphosphorylation and subsequent aggregation. Among tau kinases, Glycogen Synthase Kinase-3β (GSK3β) is particularly relevant. GSK3β can phosphorylate Tau at more than 40 sites, making it one of the most effective drivers of pathological hyperphosphorylation (Martin et al., 2013). Under normal conditions, its activity is negatively regulated by phosphorylation at Serine 9 (Ser9), typically mediated by Akt/PKB, thereby limiting phosphorylation (Planel et al., 2004). In AD, this inhibitory regulation is compromised, leading to chronically overactive GSK3β (Squarcio et al., 2023).

Interestingly, Tau hyperphosphorylation is not restricted to AD or tauopathies but also occurs under hypothermic conditions in both physiological and experimental contexts, including hibernation, deep anesthesia, and synthetic torpor (ST), pharmacologically induced hypothermic /hypomethabolic state in non-hibernators such as rats (Cerri et al., 2013; Sisa et al., 2017; Luppi et al., 2019). In these states, hyperphosphorylation is reversible and does not lead to neurodegeneration, suggesting it is part of a regulated adaptive mechanism (Planel et al., 2004; Squarcio et al., 2023). The primary driver of PP-Tau accumulation under hypothermia is the differential temperature sensitivity of GSK3\beta and protein phosphatase 2A (PP2A), with PP2A activity declining more rapidly than GSK3ß (Planel et al., 2004; Su et al., 2008). Importantly, upon return to normothermia, Tau phosphorylation rapidly normalizes, pointing to active neuroprotective mechanisms. In this context, Squarcio et al. (2023) demonstrated that ST is associated with GSK3ß inhibition, Akt activation, and elevated melatonin levels, supporting the view that hypothermia triggers a regulated biochemical program favoring PP-Tau reversibility.

Thus, ST provides a valuable model to investigate adaptive mechanisms of tau regulation under hypothermia. However, translating these protective processes into therapeutic strategies requires alternative, non-invasive interventions. One promising candidate is photobiomodulation (PBM).

PBM is a light-based, non-ionizing neuromodulatory approach using lasers or light-emitting diodes (LEDs) to stimulate cellular processes (Hamblin, 2016, 2019; Heiskanen & Hamblin, 2018; Salehpour et al., 2018; Chao, 2019). Its mechanisms involve photon absorption by cytochrome c oxidase in mitochondria (Karu, 1999), leading to increased ATP production, reduced oxidative stress, anti-inflammatory effects, and enhanced cerebral blood flow. These effects are directly relevant to AD pathology. Indeed, multiple preclinical and clinical studies have shown that PBM can reduce Aß burden, modulate Tau phosphorylation, improve cognition while decreasing and neuroinflammation (Lim, 2024; Lin et al., 2024). For example, in a pilot trial, transcranial and intranasal near-infrared PBM improved cognitive and behavioral outcomes in dementia patients, including those with AD (Chao, 2019).

Several experimental protocols specifically highlight PBM's ability to modulate Aß pathology. Transcranial PBM at 633 nm improved memory performance in AD mouse models by shifting APP processing toward the non-amyloidogenic pathway via Sirtuin 1-dependent cAMP/PKA signaling (Zhang et al., 2020). PBM at 808 nm enhanced mitochondrial function and lymphatic clearance, promoting AB removal, while even longer wavelengths (e.g., 1267 nm) activated glymphatic pathways (Huang et al., 2024a; Lin et al., 2024; Wang et al., 2024). Other studies report reduced plaque burden through enhanced microglial phagocytosis, with concomitant cognitive improvements (De Taboada et al., 2011; Saltmarche et al., 2017). However, not all findings are positive: a randomized, blinded study in an AD mouse model found no effect of PBM on cognition or histological markers (Sipion et al., 2023), underscoring protocol-dependent variability and the need for mechanistic clarification.

Compared to the numerous PBM studies on A\u03c3, fewer have examined Tau pathology. Among the limited evidence, (Purushothuman et al., 2014) reported that transcranial PBM at 670 nm (continuous wave, 4 J/cm² daily for four weeks) reduced Tau hyperphosphorylation and tangle formation in K3 transgenic mice. Moreover, (Chen et al., 2025) demonstrated that abdomen-targeted PBM (630, 730, and 850 nm, continuous wave, 100 J/cm², five days per week for eight weeks) improved memory and reduced hippocampal Aβ and Tau phosphorylation in wild-type mice infused with Aβ. These findings support the idea that PBM can influence both major hallmarks of AD, though the underlying mechanisms, particularly for Tau, remain underexplored.

In this study, we investigated a specific PBM modality: Hyperpolarized Light (HPL), also known as Quantum Hyperlight. HPL originates from diffuse halogen light that is linearly polarized and then interacts with C60 fullerene molecules embedded in a polymeric matrix. These molecules generate an icosahedral twisting structure that imposes a Fibonacci-sequential effect on photons, producing a complex polarization pattern combining circular (left- and right-handed) and linear (vertical and horizontal) components, described as a "sunflower seed photon pattern" (De Wever, 2024; Koruga, 2018). This nanophotonic process is proposed to enhance light-tissue interactions, thereby improving mitochondrial function, nitric oxide release, cerebral blood flow, anti-inflammatory responses, and tissue regeneration (BIOPTRON Hyperlight, no date; Raeissadat et al., 2014; Tian et al., 2023).

For experimental delivery, we employed the BIOPTRON MedAll, a CE-certified medical device emitting HPL across a broad spectrum (350–3400 nm) with 95% polarization and a power density of 40 mW/cm². The extended wavelength coverage into the near- and mid-infrared range allows interaction with multiple chromophores and tissue components, potentially offering therapeutic advantages over conventional PBM.

Given that both PBM and HPL effects are highly dependent on irradiation parameters, we tested multiple exposure durations to establish dose–response relationships and optimize efficacy. Our study introduces a novel therapeutic perspective by exploring the effects of HPL in rats subjected to ST-induced Tau phosphorylation. To assess these effects, we quantified Tau-1 (non-phosphorylated Tau), pGSK3β (Ser9), and p-Tau205 (tau phosphorylated at threonine 205) by Western blotting, thereby evaluating irradiation-dependent modulation of key molecular markers.

2. Materials and methods

2.1 Ethical approval

All experimental procedures were authorized by the Ethical-Scientific Committee of the University of Bologna and carried out in compliance with the European Directive 86/609/EEC. The work was conducted under the oversight of both the University's Central Veterinary Service and the Italian National Health Authority. Discomfort or pain were minimized as well as the number of animals used.

2.2 Sample preparation

Male Sprague - Dawley rats (n = 2, 300 gr) were deeply anesthetized with isoflurane (mg/mg) and decapitated. The brain was rapidly removed and meticulously in ice-cold artificial Cerebrospinal Fluid (aCSF) bubbled with 95% O2/5% CO2, containing in (nM/L): (126) NaCl, (3) KCl, (26) NaHCO3, (2) CaCl2, (1) MgSO4, (10) D-Glucose, (1.25) NaH2PO4. The solution pH was 7.4 and the osmolarity was 295 mOsm/L. The region of the brain containing the hippocampus was carefully dissected by excising both the frontal and caudal segments, resulting approximately in a rectangular section (15 mm wide, 10 mm high).

The brain tissue was fully immersed in oxygenated aCSF, maintained at 3–4 °C throughout the slicing process. Coronal brain slices (300 µm thick, n = 8 per rat) were prepared using a Vibroslice NVSLM1 vibrating microtome, with the tissue mounted on the specimen holder using superglue. Slices were then assigned to two main groups according to incubation temperature: physiological (37 °C) and room temperature (25 °C). Each group was further divided into exposed (treated) and unexposed (control) subgroups. HPLT exposure was applied for either 10 or 20 minutes, with two slices tested per condition. This same experimental design was applied for both temperature groups.

2.3 Temperature set-up

Slices in group a were maintained at physiological temperature (37 °C) using a Liquid Bath Temperature Calibrator Ambient, ensuring stable and accurate regulation of aCSF temperature. In group b, slices were initially adjusted to 37 °C before undergoing a carefully controlled cooling to 25 °C.

This process involved decreasing the temperature from 37 °C to 30 °C over 30 minutes, followed by a gradual reduction to 25 °C over one hour. Throughout cooling, samples contained in Coplin Staining Jars were immersed in a temperature-regulated bath to achieve precise thermal control. The temperature was then held steady at 25 °C for an additional hour to promote enhanced AT8 signal detection, likely reflecting sustained phosphorylation or stabilization of Tau epitopes as previously described (Luppi *et al.*, 2019; Squarcio *et al.*, 2023).

Table 1. Primary antibodies employed for Western Blotting analysis. Vinculin was used as ladder control for the analysis.

Antibody	Туре	Species	Specificity	MW (kDa)	Diluition
Anti-Tau 1	Mono	Mouse	Non-phosphorylated 189–207 residues	52-68	1:1000
Anti-p-Tau (p-205)	Mono	Rabbit	T205	68-70	1:500
Anti-p-GSK3β	Mono	Rabbit	S9	46	1:1000
Vinculin	Mono	Rabbit	Vinculin	116	1:8000

2.4 Irradiation

Samples irradiation was performed with the Bioptron MedAll device. A distance of 12.5 cm was set from the light lamp, with time intervals equal to 10 and 20 minutes respectively. Technical specifications are reported in detail in the Appendix (**Table A1 and A2**). To perform the irradiation, each brain slice was removed from the beaker and subsequently immersed in a water bath [group a (37°C), group b (25°C)]. A thermal camera was used to monitor the temperature.

2.5 Western blotting

Brain slices were homogenized by ice-assisted sonication in RIPA lysis buffer [50 mM Tris, 150 mM NaCl, 10% (v/v) NP-40, 1 mM dithiothreitol (DTT), 1 mM phenylmethylsulfonyl fluoride (PMSF) mixed with a cocktail of phosphatase and protease (Sigma Aldrich)]. The buffer formulation was optimized to ensure sample stability. The extract was centrifuged and stored at -80°C. Bio-Rad DC protein assay kit (Bio-Rad Laboratories) was used to determine protein concentration. For each lane, 20 µg of protein was loaded; samples were diluted to a final concentration of $1 \mu g/\mu L$ with H_2O , with $5 \mu L$ of loading buffer added. Samples were denatured at 65°C for 10 minutes (450 rpm), briefly centrifuged, and stored on ice until loading. SDS-PAGE was performed using 1.0 mm thick 4-12% Bis-Tris gels with NuPAGE MOPS SDS Buffer (InvitrogenTM) at a constant voltage of 100-200 V. Proteins were transferred onto nitrocellulose membranes (Hybond C Extra, Amersham Pharmacia) by wet transfer at 4°C for up to 3 hours (300 mA). Membranes were rinsed to remove excess buffer and incubated with Ponceau S solution for 1 minute at room temperature for protein visualization, followed by

distilled water to clear the background. Blocking was performed in 5% (w/v) non-fat milk in PBST for 40 minutes at room temperature. Membranes were incubated overnight at 4°C with primary antibodies (see Table 1) diluted in PBST. After three washes (10 minutes each, PBST), HRP-conjugated secondary antibodies (see Table 2) were applied for 45 minutes. Signal was visualized using a chemiluminescence reaction (ECL reagents, Amersham) and imaged with iBrightTM CL1500 Imaging System (ThermoFisher Scientific). Band intensity was semi-quantified with iBright Analysis Software. Data from different gels were normalized to a randomly selected reference sample, obtained from a single rat and loaded on every gel as an internal control across all determinations. The most representative results are shown for both Rat 1 and Rat 2 in the Appendix (Figures A1, A2 and A3).

Table 2. Secondary antibodies employed for Western Blotting analysis.

Antibody	Type	Specificity	Diluition
Anti-Mouse	Poly	Anti-Mouse	1:10000
HRP		IgG	
Anti-Rabbit	Poly	Anti-Rabbit	1:10000
HRP		IgG	

3. Results

The figures below show the four experimental conditions tested after the Bioptron MedAll device: temperature (37°C, 25°C) and time exposure (10, 20

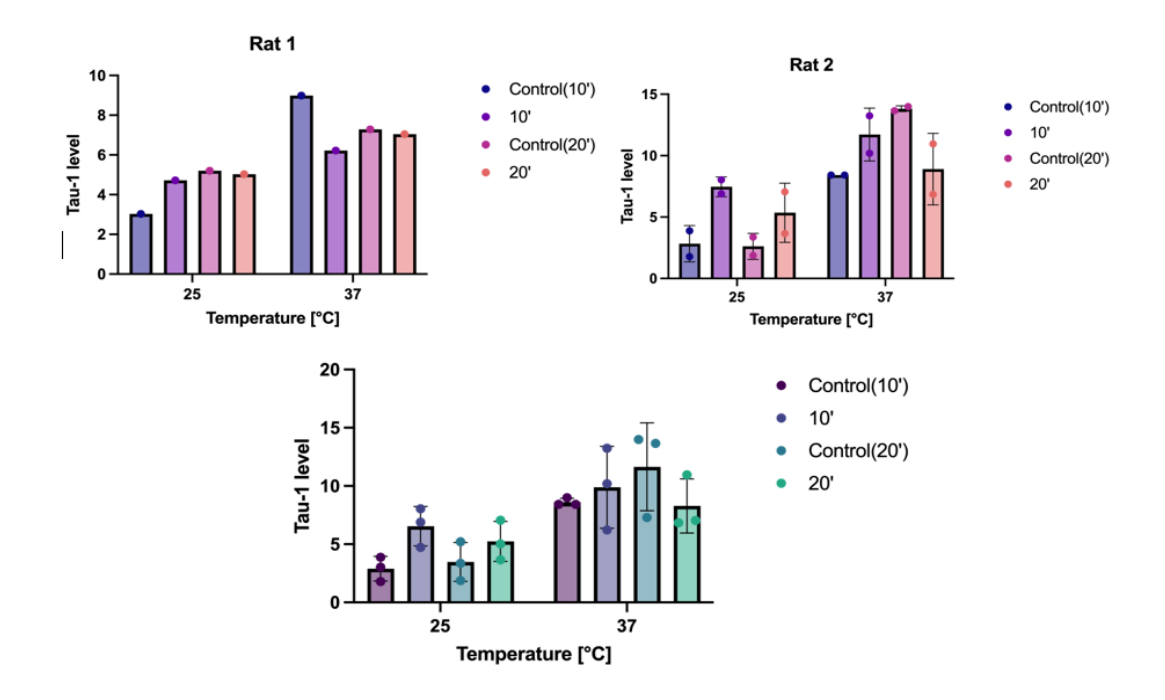


Figure 1. Representative Western blot analysis of non-phosphorylated Tau-1. Quantification of Tau-1 expression is shown separately for Rat 1 (a) and Rat 2 (b), while panel (c) presents the pooled analysis combining data from both animals. For the combined dataset, three independent replicates were considered for analyzing each experimental condition.

minutes). temperature (37°C, 25°C) and time exposure (10, 20 minutes).

1. Tau 1

Figure 1a shows the levels of Tau-1 protein measured in Rat 1. There is a decrease in Tau-1 levels after both 10- and 20- minutes of irradiation of cold samples (25°C). The same behavior is shown from the treated warm sample (37°C) with respect to the unexposed warm one after 10 minutes of irradiation. However, after 20 minutes of exposure, the Tau-1 expression in the warm samples is increased (compared to the control).

2. p-GSK3B

Under warm conditions (37 °C) in Rat 1, the duration of HPLT exposure had a notable impact on p-GSK3 β levels: a 10-minute exposure led to a substantial decrease compared to controls, whereas a 20-minute exposure produced the opposite effect, resulting in increased expression (see **Figure 2a**). In contrast, for samples maintained at 25 °C, HPLT exposure for 10 minutes markedly elevated p-GSK3 β relative to controls; however, extending the exposure to 20

minutes reversed this trend, yielding a reduction similar to that observed under warm conditions.

For Rat 2, two measurements were performed for each condition, except for the 20-minute exposures at both temperatures, which included a third replicate (**Figure 2b**). In this animal, a 10-minute exposure at 37 °C resulted in increased p-GSK3β expression compared to controls, while the same exposure at 25 °C was associated with decreased kinase phosphorylation. Prolonging HPLT exposure to 20 minutes under warm conditions further promoted p-GSK3β accumulation (three replicates).

In contrast, at 25 °C, p-GSK3β levels declined after 10 minutes of HPLT yet increased following 20 minutes of exposure. These data highlight notable interindividual variability: Rat 1 predominantly exhibited reduced p-GSK3β expression at shorter exposure times across both temperatures, while Rat 2 showed greater sensitivity to prolonged exposure, with levels tending to increase in most conditions, particularly with extended irradiation duration. The overall trend again indicated that temperature influenced the photobiomodulation effect (**Figure 2c, Table S4**).

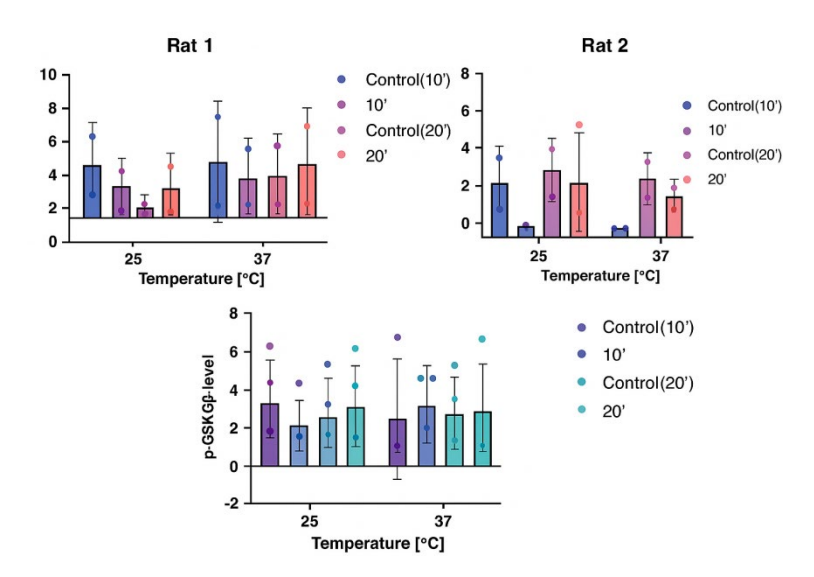


Figure 2. Representative Western blot analysis of phosphorylated GSK3β at serine 9 (p-GSK3β, Ser9). Quantification of p-GSK3β expression is shown for Rat 1 (a) and Rat 2 (b), while panel (c) presents the pooled analysis combining data from both animals. In the pooled dataset, each experimental condition was represented by four replicates, except for the 20-minute exposure condition, which included five replicates.

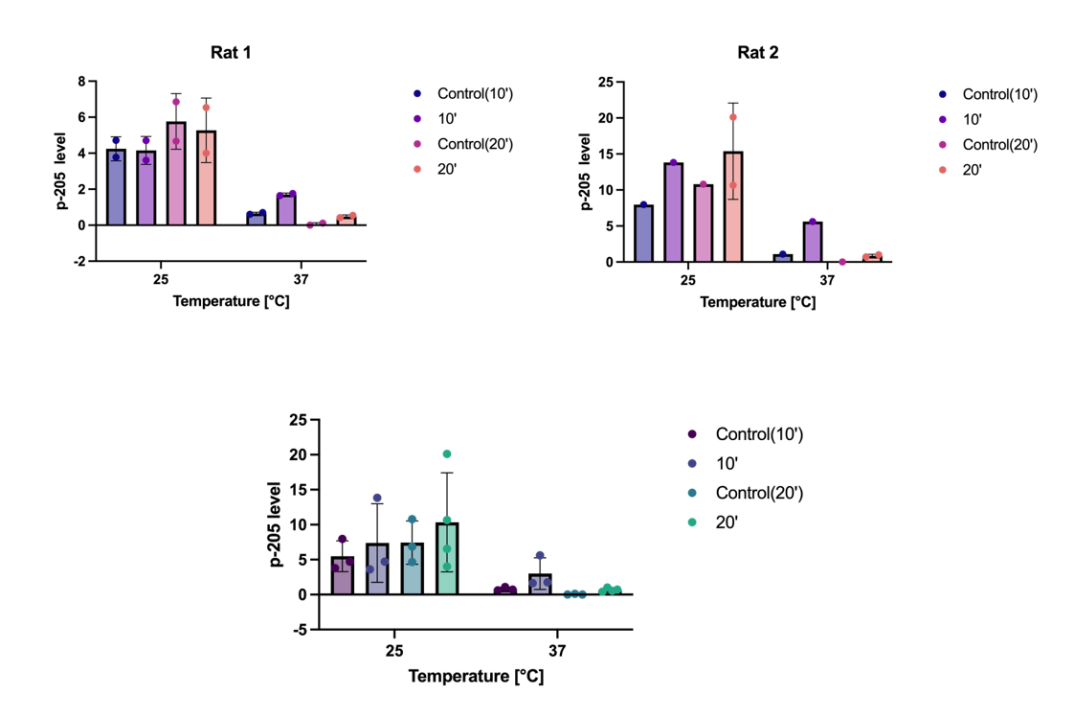


Figure 3. Representative Western blot analysis of phosphorylated Tau at threonine 205 (p-T205). Quantification of p-T205 expression is shown for Rat 1 (a) and Rat 2 (b), while panel (c) illustrates the pooled analysis combining data from both animals. In the pooled dataset, each experimental condition was represented by three replicates, except for the 20-minute exposure condition, which included four replicates.

3. p-T205

For Rat 1, two samples were analyzed per condition (**Figure 3a**). Both 10- and 20-minute HPLT exposures at 37 °C resulted in higher p-205 levels compared to their respective controls. At 25 °C, the two samples exposed for 10 minutes showed inconsistent results, while both replicates following 20 minutes of exposure demonstrated a pronounced reduction in P205 levels.

In Rat 2 (**Figure 3b**), p-205 levels were consistently elevated at both 25 °C and 37 °C following 10 minutes of HPLT, compared to the respective controls. After 20 minutes of exposure at 37 °C, p-205 levels also appeared increased; however, the corresponding control samples were unreliable, and this comparison was therefore not considered valid. Conversely, at 25 °C, 20 minutes of HPLT exposure still resulted in higher p-T205 levels relative to the control.

The comparison between the two animals reveals that Rat 2 consistently exhibited higher p-T205 levels following HPLT than Rat 1 under all tested conditions.

Notably, prolonged HPLT exposure at 37 °C (20 minutes) led to elevated p-T205 in both rats, yet no Tau phosphorylation at the T205 residue was detected in the control group for Rat 2. The overall response exhibited a consistent trend, regardless of exposure time or temperature (see **Figure 3c, Table A5**).

4. Discussion

Photobiomodulation (PBM) has emerged as a promising intervention for Alzheimer's disease (AD), owing to its ability to modulate multiple cellular processes implicated in disease progression (Huang *et al.*, 2024a). To date, most research has focused on amyloid-β (Aβ) pathology, while the effects of PBM on tau hyperphosphorylation and neurofibrillary tangle formation remain relatively underexplored. Among the few studies addressing tau, Purushothuman *et al.* (2015) demonstrated that transcranial PBM at 670 nm (continuous wave, 4 J/cm² daily for four weeks) reduced both tau hyperphosphorylation and tangle burden in K3 transgenic mice (Purushothuman *et al.*,

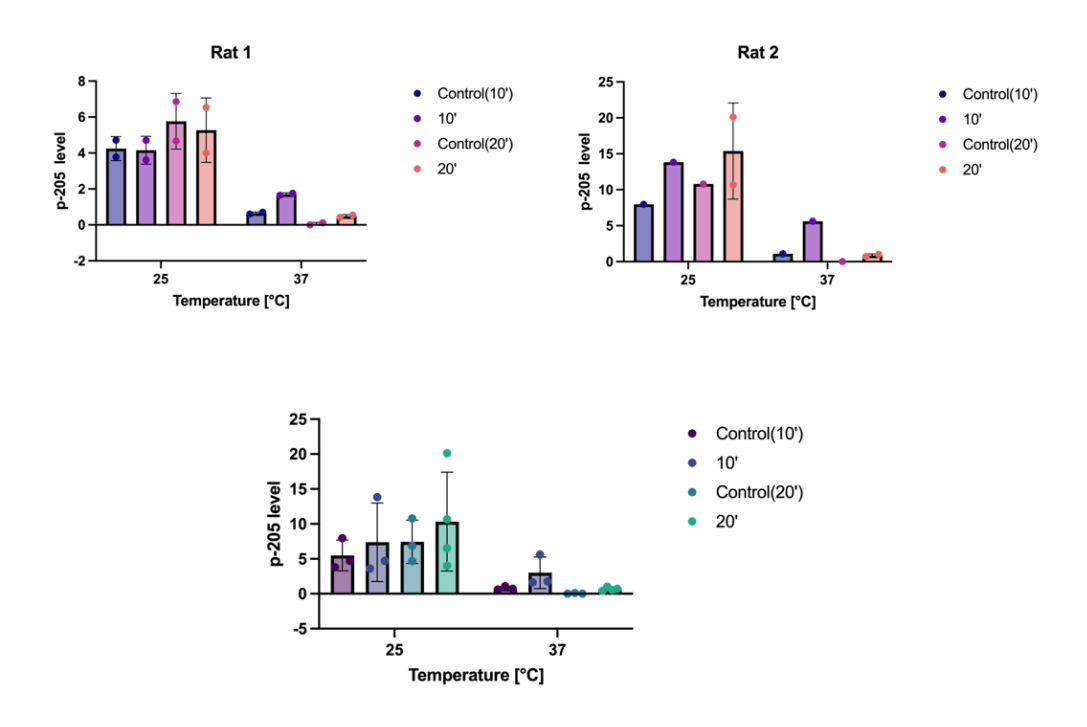


Figure 3. Representative Western blot analysis of phosphorylated Tau at threonine 205 (p-T205). Quantification of p-T205 expression is shown for Rat 1 (a) and Rat 2 (b), while panel (c) illustrates the pooled analysis combining data from both animals. In the pooled dataset, each experimental condition was represented by three replicates, except for the 20-minute exposure condition, which included four replicates.

2015). Moreover, evidence suggests that PBM applied outside the brain can modulate central pathology: in wild-type mice infused with Aβ, abdomen-targeted PBM (630, 730, and 850 nm; continuous wave, 100 J/cm², five days per week for eight weeks) improved memory and reduced hippocampal Aβ deposition and tau phosphorylation (Chen *et al.*, 2021). While PBM is known to enhance mitochondrial function, increase ATP production, and reduce oxidative stress—thereby promoting neuroprotection and neurostimulation (Hamblin, 2017; Huang *et al.*, 2024b; Ramanishankar *et al.*, 2024), its specific effects on tau remain poorly understood, highlighting a critical knowledge gap in evaluating PBM as a therapeutic strategy for AD.

The present study aimed to investigate the potential of PBM in modulating tau phosphorylation using two main innovations: (a) the induction of tau hyperphosphorylation via synthetic torpor, allowing direct assessment of PBM effects in brain slices, and (b) the use of a broad wavelength spectrum spanning the IR range with Bioptron Quantum Hyperlight (350–3400 nm). We focused on Tau-1 (non-phosphorylated tau), p-GSK3β, and p-T205, markers relevant to tau stability and phosphorylation dynamics (Saltmarche *et al.*, 2017; Huang *et al.*, 2024a; Lantero-Rodriguez *et al.*, 2024)

Tau-1 plays a crucial role in maintaining microtubule stability in neurons, whereas Glycogen Synthase Kinase-3β (GSK3β) is a principal tau kinase implicated in AD pathogenesis (Huang *et al.*, 2024a). Phosphorylation at Thr205 (p-T205) has recently emerged as a potential biomarker for tauopathy progression (Lantero-Rodriguez *et al.*, 2024). In AD, the balance between phosphorylated and non-phosphorylated tau is disrupted, shifting toward hyperphosphorylation and formation of neurofibrillary tangles (Lim, 2024).

To model reversible tau hyperphosphorylation, we used a synthetic torpor approach in rat brain slices. By lowering the incubation temperature to 25 °C, we transiently slowed cellular metabolism and enzymatic kinetics, producing a controlled, reversible increase in phosphorylated tau (PP-Tau) to mimic torpor- or hibernation-associated changes without causing permanent pathology (Planel *et al.*, 2007; Cerri *et al.*, 2021). Warm slices (37 °C) were used as physiological controls, allowing us to compare PBM effects under normothermic and hypometabolic conditions.

Our study demonstrates that photobiomodulation (PBM) delivered as high-polarized light (HPL) can

modulate tau biology on top of a synthetic-torpor baseline. The strongest and most consistent effects were observed in warm slices (37 °C), where mitochondrial and enzymatic activity remain intact. In these slices, Tau-1 levels, the non-phosphorylated form crucial for microtubule stability, increased following both 10- and 20-minute exposures, particularly in rat 2, suggesting a shift toward a less hyperphosphorylated, more physiological tau state (Saltmarche *et al.*, 2017).

Mechanistically, PBM stimulates mitochondrial cytochrome c oxidase (CCO), transiently enhancing ATP production, modulating reactive oxygen species (ROS), and activating the PI3K/Akt pathway (Hamblin, 2017; Salehpour et al., 2018). Akt activation phosphorylates GSK3\beta at Ser9, reducing its kinase activity and thereby lowering tau phosphorylation (Squarcio et al., 2023; Huang et al., 2024a). GSK3β functions as a central integrator of both metabolic and phosphorylation signals, acting as a metabolic sensor that links energy status with tau regulation (Hooper et al., 2008; Beurel et al., 2015). PBM acts on this node through Akt-mediated inhibition, promoting Tau-1 accumulation. However, under hypothermic, torporlike conditions (25 °C), the overall enzymatic activity is reduced and phosphatases such as PP2A are more temperature-sensitive, blunting PBM's impact on GSK3β and tau dephosphorylation (Planel et al., 2007, 2009; Cerri et al., 2013). This explains the smaller and more variable effects observed in cold slices and illustrates why tau phosphorylation in torpor resembles early AD yet remains fully reversible upon rewarming (Cerri et al., 2021)

The phosphorylation signal at Thr205 (p-T205) displayed site-specific variability. In warm slices, p-T205 increased after 20 minutes of HPL, whereas cold slices showed inconsistent results between animals. This pattern likely reflects multiple mechanisms: (1) Thr205 phosphorylation can be mediated by kinases beyond GSK3\(\beta\), including CDK5 and stress-activated MAPKs, which may transiently compensate under PBM-induced signaling(Noble et al., 2003; Reynolds et al., 2008) and (2) PBM-induced ROS/redox signaling can transiently activate stress kinases, producing short-term increases at specific phosphoepitopes even while global tau phosphorylation decreases(Iliff et al., 2012; Butterfield & Boyd-Kimball, 2018; Zubčić et al., 2020). These observations support a model in which PBM shifts the overall tau phosphorylation balance toward a less pathological state (increase in Tau-1), while allowing transient, siteand dose-specific fluctuations in p-T205.

In addition to direct modulation of tau phosphorylation, PBM may facilitate metabolic waste clearance through glymphatic system activation (Patel et al., 2019). In sleep-like or hypometabolic states, PBM could enhance cerebrospinal-interstitial fluid exchange, potentially via aquaporin-4 channel modulation on astrocytic endfeet, promoting removal of tau and other metabolites (Iliff et al., 2012; Xie et al., 2013). While this mechanism remains speculative in the ex vivo context, it provides a plausible complementary pathway through which PBM could protect neuronal function, particularly under conditions where kinase/phosphatase dynamics are slowed hypothermia.

Several factors limit the interpretation of our results. Cooling slices to simulate torpor bypasses systemic thermoregulatory mechanisms and the dimensional architecture of the brain, preventing analysis of cerebrospinal fluid dynamics and water structure, particularly relevant for PBM given the role of nanostructured water in light-tissue interactions and the overlap of extended wavelengths (>900 nm) with water absorption bands (Pollack & Reitz, 2001; Pollack, 2003; Trevors & Pollack, 2012; Hamblin, 2019). The small number of slices and use of only two animals precluded statistical analysis, so findings should be interpreted as preliminary and descriptive. Inter-individual variability further limits generalizability. Finally, some mechanistic interpretations, particularly regarding glymphatic-like waste clearance, remain speculative but offer a framework for future in vivo studies exploring HPL/PBM in neurodegeneration.

Taken together, our findings indicate that PBM delivered as HPL can modulate tau biology, but the magnitude and direction of effects are strongly dependent on slice temperature, PBM dose, and exposure duration. Warm slices consistently exhibited Tau-1 increases and trends toward reduced pathological phosphorylation, whereas cold slices showed smaller, more heterogeneous responses. These results emphasize two practical points for interpretation: (i) PBM can produce nonlinear, site-specific effects on tau phosphorylation depending on dose and exposure time; and (ii) pharmacological (e.g., Akt or PP2A inhibitors) or thermal dissections are recommended to distinguish true PBM signaling from temperature-dependent or thermal artifact effects.

5. Conclusions

The study demonstrates that hyperpolarized light (HPL) can modulate tau phosphorylation in an ex vivo rat brain slice model of reversible, torpor-induced tau hyperphosphorylation. HPL effects were strongly temperature- and dose-dependent: warm slices (37 °C) consistently showed increased non-phosphorylated Tau-1 and trends toward reduced pathological phosphorylation, while cold slices (25 °C) exhibited more variable and attenuated responses. HPL appears to shift tau homeostasis toward a less pathological state, possibly through mitochondrial support and partial inhibition of GSK3β. At the same time, the transient and site-specific increases in certain phospho-epitopes (e.g., p-T205) highlight the intricate and non-linear dynamics of tau phosphorylation. While these results suggest a promising role for HPL in modulating tau biology, the limited number of slices, use of only two animals, and the ex vivo setting preclude generalization. Further studies will be essential to confirm these preliminary observations and to evaluate the therapeutic potential of HPL/PBM for developing future neuroprotective interventions.

Acknowledgments

The authors acknowledge the support of the Zepter Group (Switzerland), which provided the Bioptron MedAll device employed in the experiments.

Conflict of Interest Statement

All authors declare no conflict of interest.

Bibliography

Avila, J. (2006) Tau phosphorylation and aggregation in Alzheimer's disease pathology. *FEBS Letters* **580**, 2922–2927.

Beurel, E., Grieco, S.F. & Jope, R.S. (2015) Glycogen synthase kinase-3 (GSK3): Regulation, actions, and diseases. *Pharmacology & Therapeutics* **148**, 114–131.

BIOPTRON (n.d.) Hyperlight. Available at: https://www.bioptron.com/how-it-works/bioptron-hyperlight-therapy/

Butterfield, D.A. & Boyd-Kimball, D. (2018) Oxidative stress, amyloid-β peptide, and altered key molecular pathways in the pathogenesis and progression of Alzheimer's disease. *Journal of Alzheimer's Disease* **62**, 1345–1367.

Calabrò, M., Rinaldi, C., Santoro, G., & Crisafulli, C. (2021) The biological pathways of Alzheimer disease: a review. *AIMS Neuroscience* **8**, 86–132.

- Cerri, M., Mastrotto, M., Tupone, D., Martelli, D., Luppi, M. et al. (2013) The inhibition of neurons in the central nervous pathways for thermoregulatory cold defense induces a suspended animation state in the rat. *Journal of Neuroscience* **33**, 2984–2993.
- Lin, H., Li, D., Zhu, J., Liu, S., Yu, T. et al. (2024) Transcranial photobiomodulation for brain diseases: review of animal and human studies including mechanisms and emerging trends. *Neurophotonics* **11**, 010601.
- Luppi, M., Hitrec, T., Di Cristoforo, A., Squarcio, F., Stanzani, A. et al. (2019) Phosphorylation and dephosphorylation of tau protein during synthetic torpor. *Frontiers in Neuroanatomy* **13**, 57
- Martin, L., Latypova, X., Wilson, C., Magnaudeix, A., Perrin, M. et al. (2013) Tau protein kinases: Involvement in Alzheimer's disease. *Ageing Research Reviews* **12**, 289–309.
- Noble, W., Olm, V., Takata, K., Casey, E., Mary, O. et al. (2003) Cdk5 is a key factor in tau aggregation and tangle formation *in vivo*. *Neuron* 38, 555–565.
- Patel, T.K., Habimana-Griffin, L., Gao, X., Xu, B., Achilefu, S. et al. (2019) Dural lymphatics regulate clearance of extracellular tau from the CNS. *Molecular Neurodegeneration* **14**, 11.
- Planel, E., Miyasaka, T., Launey, T., Chiu, D., Tanemura, K. et al. (2004) Alterations in glucose metabolism induce hypothermia leading to tau hyperphosphorylation through differential inhibition of kinase and phosphatase activities: Implications for Alzheimer's disease. *Journal of Neuroscience* **24**, 2401–2411.
- Planel, E., Richter, K., Nolan, C., Finley, J., Liu, L. et al. (2007) Anesthesia leads to tau hyperphosphorylation through inhibition of phosphatase activity by hypothermia. *Journal of Neuroscience* **27**, 3090–3097.
- Planel, E., Bretteville, A., Liu, L., Virag, L., Du, A. et al. (2009) Acceleration and persistence of neurofibrillary pathology in a mouse model of tauopathy following anesthesia. *The FASEB Journal* **23**, 2595–2604.
- Pollack, G.H. (2003) The role of aqueous interfaces in the cell. *Advances in Colloid and Interface Science* **103**, 173–196.
- Pollack, G.H. & Reitz, F.B. (2001) Phase transitions and molecular motion in the cell. *Cellular and Molecular Biology (Noisy-le-Grand, France)* **47**, 885–900.
- Purushothuman, S., Johnstone, D., Nandasena, C., Mitrofanis, J. & Stone, J. (2014) Photobiomodulation with near infrared light mitigates Alzheimer's disease-related pathology in cerebral cortex evidence from two transgenic mouse models. *Alzheimer's Research & Therapy* **6**, 2.
- Purushothuman, S., Johnstone, D., Nandasena, van Eersel, J., C., Ittner, L. et al. (2015) Near infrared light mitigates cerebellar pathology in transgenic mouse models of dementia. *Neuroscience Letters* **591**, 155–159.

- Hamblin, M.R. (2017) Mechanisms and applications of the anti-inflammatory effects of photobiomodulation. *AIMS Biophysics* **4**, 337–361.
- Raeissadat, S.A., Rayegani, S.M., Rezaei, S., Sedighipour, L. Bahrami, M.H. et al. (2014) The effect of polarized polychromatic noncoherent light (Bioptron) therapy on patients with carpal tunnel syndrome. *Journal of Lasers in Medical Sciences* 5, 39-46.
- Ramanishankar, A. et al. (2024) Unleashing light's healing power: an overview of photobiomodulation for Alzheimer's treatment. *Future Science OA* 10(1).
- Reynolds, C.H. et al. (2008) Phosphorylation regulates tau interactions with Src homology 3 domains of phosphatidylinositol 3-kinase, phospholipase Cγ1, Grb2, and Src family kinases. *Journal of Biological Chemistry* **283**, 18177–18186.
- Salehpour, F. et al. (2018) Brain photobiomodulation therapy: a narrative review. *Molecular Neurobiology* **55**, 6601–6636.
- Saltmarche, A.E., Naeser, M., Ho, K., Hamblin, M. & Lim, L. (2017) Significant improvement in cognition in mild to moderately severe dementia cases treated with transcranial plus intranasal photobiomodulation: Case series report. *Photomedicine and Laser Surgery* **35**, 432–441.
- Sergeant, N., Bretteville, A., Hamdane, M, Caillet-Boudin, M., Grognet, P. et al. (2008) Biochemistry of tau in Alzheimer's disease and related neurological disorders. *Expert Review of Proteomics* 5, 207–224.
- Sipion, M., Ferreira, F., Scholler, J., Brana, C., Gora, M. et al. (2023) A randomized, blinded study of photobiomodulation in a mouse model of Alzheimer's disease showed no preventive effect. *Scientific Reports* **13**, 19828.
- Sisa, C., Turroni, S., Amici, R., Brigidi, P., Candela, M. et al. (2017) Potential role of the gut microbiota in synthetic torpor and therapeutic hypothermia. *World Journal of Gastroenterology* 23, 406.
- Squarcio, F., Hiltrec, T., Piscitiello, E., Cerri, M., Giovannini, C. et al. (2023) Synthetic torpor triggers a regulated mechanism in the rat brain, favoring the reversibility of tau protein hyperphosphorylation. *Frontiers in Physiology* **14**, 1129278.
- Su, B., Wang, X., Drew, K., Perry, G., Smith, M. et al. (2008) Physiological regulation of tau phosphorylation during hibernation. *Journal of Neurochemistry* **105**, 2098–2108.
- De Taboada, L., Yu, J., El-Amouri, S., Gattoni-Celli, S., Richieri, S. et al. (2011) Transcranial laser therapy attenuates amyloid-β peptide neuropathology in amyloid-β protein precursor transgenic mice. *Journal of Alzheimer's Disease* **23**, 521–535.
- Tian, H., Zhu, H., Gao, C., Shi, M., Yand, D. et al. (2023) System-level biological effects of extremely low-frequency electromagnetic fields: an in vivo experimental review. *Frontiers in Neuroscience* 17,1247021.

Trevors, J.T. & Pollack, G.H. (2012) Origin of microbial life hypothesis: a gel cytoplasm lacking a bilayer membrane, with infrared radiation producing exclusion zone (EZ) water, hydrogen as an energy source and thermosynthesis for bioenergetics. *Biochimie* **94**, 258–262.

Wang, M., Yan, C., Li, X., Yang, T., Wu, S. et al. (2024) Non-invasive modulation of meningeal lymphatics ameliorates ageing and Alzheimer's disease-associated pathology and cognition in mice. *Nature Communications* **15**, 1453.

Wang, Y. & Mandelkow, E. (2016) Tau in physiology and pathology. *Nature Reviews Neuroscience* 17, 22–35.

De Wever, B.W.M. (2024) La luminothérapie Hyperlight.

Xie, L., Kang, H., Xu, Q., Chen, M., Liao, Y. & al. (2013) Sleep drives metabolite clearance from the adult brain. *Science* **342**, 373–377.

Zhang, Z., Shen, Q., Wu, X., Zhang, D., & Xing, D. (2020) Activation of PKA/SIRT1 signaling pathway by photobiomodulation therapy reduces $A\beta$ levels in Alzheimer's disease models. *Aging Cell* **19**, e13054.

Zubčić, K., Hof, P., Šimić, G., & Jazvinšćak Jembrek, M. (2020) The role of copper in tau-related pathology in Alzheimer's disease. *Frontiers in Molecular Neuroscience* **13**, 572308.

Appendix: Supplementary material

Table A3. Summary of Tau-1 values detected by Western blotting. Values were calculated using data from both Rat 1 and Rat 2. SD indicates standard deviation, N indicates the number of replicates, and MSE indicates mean squared error.

Mean	SD	N	MSE
8,61	0,33	3	0,19
2,90	1,05	3	0,61
9,89	3,52	3	2,03
6,55	1,69	3	0,97
11,64	3,78	3	2,18
3,48	1,67	3	0,96
8,29	2,32	3	1,34
5,24	1,71	3	0,99

Table A1. Technical Specifications Bioptron MedAll Device.

Parameter	Value
Wavelength	350-3400 nm
Degree of Polarization	>95%
Specific Power Density	av. 40 mW/cm ²
Light Energy per minute	av. 2.4 J/cm ²
Voltage	100-240 V
Power Consumption	75 W
Setting Therapy Time	Yes

Table A2. Manufacturer's explanation of how Bioptron's light works.

Characteristics	Description
Polarization	Its waves move on parallel planes. Polarization reaches a degree of approximately 95%, due to the presence of the Brewster Mirror Optical System.
Polychromy	Polychromatic light is used, spanning a broad range of wavelengths that encompass the visible spectrum and extend into the infrared region, while being free of ultraviolet (UV) components.
Incoherency	The device emits incoherent light, meaning the light waves are not phase-synchronized.
Low-energy	This device light has a low-energy density (fluence) of an average 2.4 J/cm ² , safe and consistently tested.
	Source: https://www.bioptron.com/how-it-works/bioptron-hyperlight-therapy/

Table A4. Summary of p-205 values detected by Western blotting. Values were calculated using data from both Rat 1 and Rat 2. SD indicates standard deviation, N indicates the number of replicates, and MSE indicates mean squared error.

Mean	SD	N	MSE
0,80	0,25	3	0,15
5,49	2,20	3	1,27
3,01	2,26	3	1,30
7,38	5,61	3	3,24
0,04	0,06	3	0,04
7,44	3,10	3	1,79
0,67	0,25	4	0,13
10,33	7,08	4	3,54

Table A5. Summary of p-T205 values detected by Western blotting. Values were calculated using data from both Rat 1 and Rat 2. SD indicates standard deviation, N indicates the number of replicates, and MSE indicates mean squared error.

Mean	SD	N	MSE
2,04	3,02	4	1,51
3,13	2,27	4	1,14
2,76	1,72	4	0,86
1,43	1,40	4	0,70
2,47	1,65	4	0,83
2,38	1,80	4	0,90
2,28	2,17	5	0,97
2,80	2,11	5	0,94

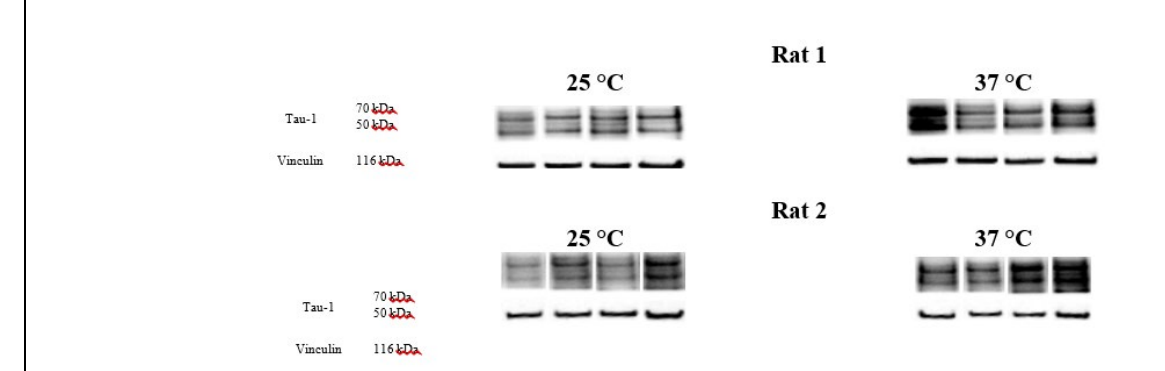


Figure A1. Western Blotting Gels indicating Tau-1 expression. Vinculin (116 kDa) was used as the loading control. The images presented correspond to the most representative results.

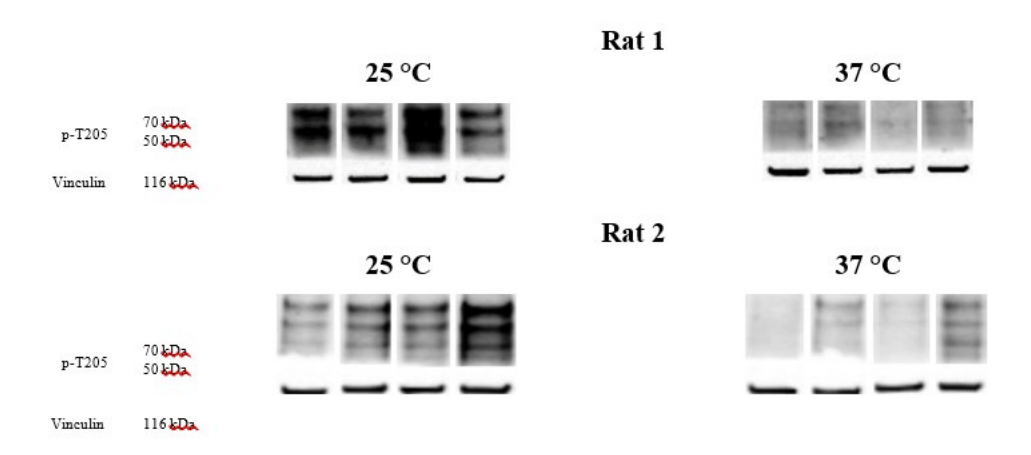


Figure A2. Western Blotting Gels indicating p-T205 expression. Vinculin (116 kDa) was used as the loading control. The images presented correspond to the most representative results.

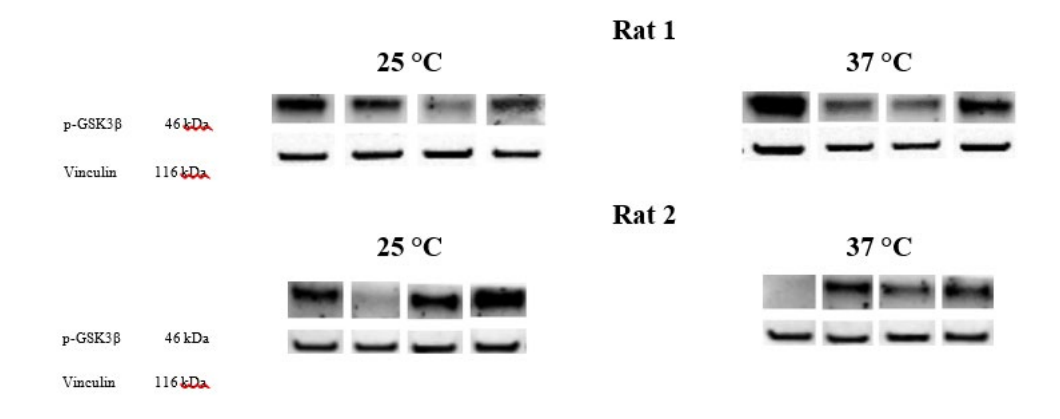


Figure A3. Western Blotting Gels indicating p-GSK3 β expression. Vinculin (116 kDa) was used as the loading control. The images presented correspond to the most representative results.